

CHAPTER 5

METAMORPHIC EVOLUTION OF THE ALUMINOUS GRANULITE

The key minerals of the aluminous granulite are spinel (Spl), ilmenite (Ilm), magnetite (Mag), garnet (Grt), sillimanite (Sil), corundum (Crn), quartz (Qtz), K-feldspar (Kfs), plagioclase (Pl) and biotite (Bt). Mineral assemblage of this rock occur as strongly deformed (few cm- to mm-thick) melanocratic and leucocratic layers. The melanocratic layers are dominantly composed of Spl-Crn-Grt-Ilm that are engulfed within quartzofeldspathic leucocratic layers (Figs. 5.1a, b) giving a migmatitic appearance of the rock. Based on the mineralogy the melanocratic layers are designated as the aluminous layers in the present study. It is important to note that the Spl-Crn-Grt bearing micro-domains of these aluminous layers locally contain Qtz, Kfs and Bt. However, there are domains where Kfs and matrix Bt are totally absent. Modal amount of Pl is low (~1%) in this rock. Zircon (Zrn) and monazite (Mnz) occur as accessory minerals. Variations in modal abundances and grain sizes of these mineral phases are noteworthy at places.

5.1 EPMA methodology

The chemical compositions of representative minerals in the aluminous granulite and the migmatitic felsic gneiss were determined using a JEOL JXA 8200 Electron Probe Micro Analyzer (EPMA) at the Natural Science Center for Basic Research and Development (N-BARD), Hiroshima University, Japan. Operating condition was 15 kV accelerating voltage, 15 nA beam current and 1–2 μm beam diameter. Natural silicate and oxide standards were used for calibration in both instruments and the raw data were corrected using the ZAF program. Fluorine contents in biotite were measured using natural fluorapatite as a standard [details have been

given by Das et al. (2017b)]. Representative mineral compositions in the aluminous granulite and the migmatitic felsic gneiss are given in Table 5.1.

5.2 Petrography and mineral chemistry of aluminous layers

Depending on the presence of K-feldspar and matrix biotite, the aluminous layers are subdivided into two mineral associations. Abbreviations for minerals are followed after Kretz (1983).

Association A is characterized by Spl, Ilm, Grt, Qtz, Kfs, Crn, Sil, Pl and Bt. Alternate layers of Grt-Spl-Crn-Ilm-Sil±Bt and Qtz-Kfs-Pl±Sil±Bt define the gneissic foliation (S_2/S_3). Porphyroblastic spinel (Spl₁) layers show micro-folding that is conformable to the outcrop-scale F_3 folds (Fig. 5.1c). Size of the Grt porphyroblasts (Grt₁) goes up to 700 µm along the maximum dimension. Porphyroblastic Crn (Crn₁) grains are usually rectangular in shape and coexist with porphyroblastic Spl (Spl₁) and Ilm (Ilm₂) sharing straight boundaries (Fig. 5.1d). Kfs grains constitute a monomineralic aggregate that locally shows pinching and swelling along the S_2/S_3 foliation. Inclusions of early Sil (Sil₁) and Bt (Bt₁) are present within Crn₁, Spl₁ and Grt₁. Locally, these inclusions show a folded internal foliation (S_1). Grt₁ also contains inclusions of Kfs and Ilm₁. Occasionally, close association of matrix Kfs and Grt₁ with partial engulfing of the former into the latter suggests that Kfs participated in garnet forming reaction. Sil₁ inclusions within Spl₁ sometimes contain inclusions of Kfs (Fig. 5.1e). Few Grt₁ grains contain rare inclusions of rounded Qtz. Coarse prismatic Sil grains (Sil₂) occur in the matrix. Skeletal intergrowth of Spl (Spl₂) and Qtz is developed over Grt₁ and Sil₂ grains (Fig. 5.1f) within the Grt-Spl-Crn-Ilm-Sil±Bt layer. A double-layer corona of Sil (Sil₃) and Grt (Grt₂) separates the Spl₁ and Spl₂ from the matrix Qtz (Figs. 5.1f, g). At places, corona of Grt₂ occurs around prismatic Sil₂ (Fig. 5.1e). Notably, the latter corona is only present in the vicinity of Spl₁ and

Spl₂. Apart from the porphyroblastic variety, fine granular and vermicular Crn (Crn₂) lamellae are also present within Spl₁/Spl₂ (inset of Fig. 5.1e) and Grt₂ respectively. In the first case, Crn₂ granules occur along the transverse fractures of Spl₁/Spl₂. Thin film of Kfs is present along the grain contacts of Sil₂ and Qtz in the matrix. Intergrown Bt (Bt₂) and Sil (Sil₄) locally wrap Grt₁ forming the S₂/S₃ fabric. Locally, Grt₁ grains show flattening parallel to the S₂/S₃ fabric implying high ambient temperature during the fabric development. The S₂/S₃ foliation is overprinted by the S₄ fabric, which at places, is transformed into a mylonitic S_{4S} fabric. The double-layer corona of Sil₃ and Grt₂ in such a case shows extreme stretching along the S_{4S} mylonitic foliation forming thread like structure (inset of Fig. 5.1g). S-C fabric is observed in planar sections cut parallel to the stretching lineation and perpendicular to the S_{4S} mylonitic foliation. Oriented grains of Sil₄, Bt₂ and stretched corona of Grt₂+Sil₃ constitute the C fabric whereas recrystallized quartz grains constitute the S fabric.

Association B is devoid of Kfs, Pl and matrix Bt with very low modal proportion of Qtz. It constitutes meter to centimeter-scale lenses within association A. Corundum grains show two modes of occurrences: (1) porphyroblastic Crn₁ with inclusions of fibrous Sil₁ and Bt₁ (Fig. 5.1h), and (2) exsolved Crn₃ with Mag and Ilm₂ in a tripartite Spl-Ilm-Mag grain (Fig. 5.1i). Spl shows broadly four modal occurrences: (1) coarse porphyroblastic Spl (Spl₁) commonly associated with Ilm₂ (Fig. 5.1i) as a part of the peak Fe-Ti-Mg-Al spinel solid solution. Granular and dendritic exsolved lamellae of Mag are found within these spinel grains, (2) Small amoeboid Spl₁ grains within Grt₁ (Fig. 5.1j), possibly formed during the prograde stage, (3) porphyroblastic Spl₂ intergrown with Sil₂ replacing Crn₁ (Fig. 5.1k) and (4) delicate vermicular to acicular Spl grains (Spl₃) within Grt₁, possibly pseudomorphing Sil₁ inclusions (Fig. 5.1l).

In both the associations, porphyroblastic Crn₁ is separated from the matrix Qtz by thin corona of Sil₃ (Fig. 5.1m). A double-layer corona of Sil₃ and Grt₂ is also present at the contact between Crn₁ and matrix Qtz (Fig. 5.1n).

Grt grains of the aluminous granulite are characterized by compositional variations only in almandine and pyrope contents with negligible spessartine and grossular contents (Table 5.1). The almandine content of garnet grains (both Grt₁ and Grt₂) in association A varies between 68-79 mole%. Grt₁ has almandine content in the range of 68-79 mole% and Grt₂ has almandine content in the range of 69-77 mole%. Slight enrichment of the pyrope content in Grt₂ (19-22 mole%) with respect to Grt₁ (15-16 mole%) within the same sample of association A is notable (see Table 5.1). Garnet grains in association B (both Grt₁ and Grt₂) are slightly Mg-rich with respect to those of association A (68-71 mole% almandine).

All the textural varieties of Spl are compositionally solid solution of hercynite and spinel with very minor gahnite component (1- 2 wt% ZnO). In porphyroblastic Spl₁, the calculated hercynite components ($X_{\text{Fe}} \times 100$) are 73-83 mole% and 66-71 mole% in associations A and B respectively (Table 5.1). All the grains are characterized by low $X_{\text{Fe}^{3+}} [= \text{Fe}^{3+}/(\text{Fe}^{2+} + \text{Fe}^{3+})]$ within the range of 0.07-0.12 in association A and 0.10-0.14 in association B indicating the presence of low magnetite component. Spl₁ grains within Grt₁ of association A have slightly higher ZnO content (2.1-2.3 wt%) compared to the other porphyroblastic Spl₁ grains. Spl₂ grains are slightly Mg-rich with respect to the Spl₁ grains of association A (70-72 mole% hercynite). $X_{\text{Fe}^{3+}}$ of these Spl₂ grains varies within the range of 0.12-0.16.

Coarse Ilm grains (Ilm₂) are characterized by low to moderate hematite content ($X_{\text{Fe}^{3+}} \times 100$) (7-12 mole% in association A and 5-14 mole% in association B). Geikelite component of these grains (both association A and association B) is low (1-3 mole%). However Ilm₁ inclusions

within Grt₁ have higher hematite content (18 mole%) relative to Ilm₂. Geikelite component in these grains is approximately 3 mole%.

In association A, Bt₁ within Spl₁ and Grt₁ are relatively Mg-rich ($X_{Mg} = 0.64-0.75$) compared to the matrix biotite (Bt₂) ($X_{Mg} = 0.63-0.67$). The TiO₂ content in Bt₁ and Bt₂ ranges within 1.78 wt% and 5.15 wt% respectively. F contents range up to 3.22 wt% and 3.05 wt% for Bt₁ and Bt₂ respectively (Table 5.1).

Crn₁ in both associations of aluminous granulites are nearly pure with minor Fe₂O₃ (~0.88 wt% in association A and ~0.81 wt% in association B). Sil grains with different textural modes have variable Fe₂O₃ content within the range of 0.54-1.0 wt%. In association A, orthoclase component of Kfs varies between 88 to 90 mole%.

5.3 Petrography and mineral chemistry of quartzofeldspathic layers

Thick quartzofeldspathic layers surrounding the aluminous domains (Association A) contain coarse grains of Qtz, Kfs and Pl. All the minerals in this layer show variable effects of deformation. In the sheared variety of aluminous granulite, these minerals show mylonitic fabric along the S₄₅ foliation. This mylonitic fabric is defined by recrystallized Qtz and Kfs grains. It is important to note that although the Qtz grains are dominantly deformed by subgrain rotation recrystallization, the Kfs grains are deformed by grain boundary migration. Minerals in this layer show textures of melt crystallization, viz. thin film of Qtz around matrix Sil₂, Kfs envelope over Pl (Figs. 5.1o, p, q) and cusped nature of Qtz grains having low dihedral angle. Development of crystal faces of Sil and Pl against Qtz are common and such texture is also interpreted to represent melt crystallization. Based on the mineralogy, the composition of the melt could be identified as granitic.

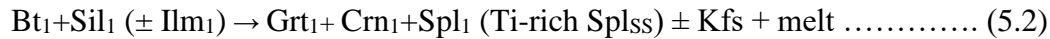
The enclosing migmatitic felsic gneiss is composed of Qtz, Kfs, Pl and porphyroblastic Grt with minor amounts of Pl and shows microstructures of shearing quite similar to that of the quartzofeldspathic layers within the aluminous granulite. S-C structure is present sporadically within this rock. The S fabric is defined by elongated Qtz grains showing recrystallization by subgrain rotation while the C fabric is defined by elongated feldspar and aggregate of Bt and Sil grains formed after porphyroblastic Grt (Fig. 5.1r). Kfs grains are elongated parallel to the mylonitic foliation (S_{4S}) and show recrystallization by grain boundary migration. Sense of shearing is sinistral as determined from the orientation of the S-C surface and the asymmetric tails of Bt and Sil aggregate around Grt. Inclusions of Bt, Qtz and Kfs are common within porphyroblastic Grt. zircon, ilmenite and apatite constitute the accessory phases of this rock.

Grt grains of the migmatitic felsic gneiss coexisting with the migmatitic variety of association A are Fe-rich (almandine 78-81 mole%; Table 5.1). These grains show diffusion zoning with minor rim-ward increase of the almandine and concomitant decrease of the pyrope components. Matrix Bt grains are Fe-rich ($X_{Mg} = 0.46-0.58$) compared to those of the aluminous granulite. TiO_2 content of these grains ranges up to 3.80 wt%. Pl grains are albitic (57-60 mole% albite).

5.4 Evolution of the mineral assemblages

Mineral assemblages, key textural features and the reactions among the mineral phases of the aluminous granulite and the migmatitic felsic gneiss are summarized in Table 5.2. In both the mineral associations of the aluminous granulite, inclusion trails (S_1) of Bt_1 , Sil_1 , and/or Ilm_1 are present within Grt_1 and Crn_1 . Rare quartz inclusions are also present in a few Grt_1 grains. These textures indicate that the prograde mineral assemblage was constituted of Bt_1 (X_{Mg} : 0.64-0.75),

Sil₁ and Ilm₁ (17-18 mole% hematite content) with rare Qtz in an overall Si-undersaturated bulk composition. This assemblage (M₁) produced the porphyroblastic phases at the pre-peak stage (pre-M₂). The transformation of M₁ to pre-M₂ stage occurred through biotite dehydration melting reactions.



Given the abundance of Crn₁, Spl₁ (hercynite: 73-83 mole% in association A, and 66-71 mole% in associations B) and Grt₁ (almandine: 68-79 mole% in association A, and 68-71 mole% in association B), it is considered that these reactions progressed to a large extent. Both the reactions occurred in an overall Si-undersaturated bulk composition, although trace amount of Qtz could have been present as the reactant phase in reaction (5.1). Kfs (orthoclase: 88-90 mole%) aggregates in association A possibly represent the peritectic phase in reactions (5.1) and (5.2). Absence of Kfs in association B implies either the phase was not produced in reaction (5.2), or if produced, was totally fractionated. The first possibility has been described in Sengupta et al. (1999), in which case the K₂O/H₂O ratio was perfectly balanced by the coexisting biotite and melt phase. Total fractionation of Kfs requires selective removal of this phase by melt, which seems quite unlikely. The chemistry of the melt produced by both the reactions is uncertain as there is practically no data on partial melting of Si-undersaturated bulk composition. However, Kelsey et al. (2005) considered such melt composition to be granitic in their theoretical modeling. Experimental data suggest that biotite dehydration melting occurs at 750-800°C at mid- to deep crustal conditions for model pelite bulk (Carrington and Harley, 1995 and references therein). In presence of high Ti and F contents in biotite (as in the present case), the melting temperature can go up to 900°C (Dooley and Patino Douce, 1995; Bose et al., 2005). The

restitic nature of the aluminous granulite implies that substantial melt-loss occurred subsequently (White et al., 2002). As a consequence of melt loss, the chemical system may change to a near-closed one which would have important consequences as discussed later. Relatively high ZnO content (up to 2.31 wt%) in the included variety of Spl₁ implies its stability below the peak temperature.

Intergrowth of Spl₂ + Sil₂ replacing Crn₁ and the development of prismatic Sil₂ surrounding Grt₁ (Fig. 5.1k) in both the mineral associations indicate a simple FMAS reaction

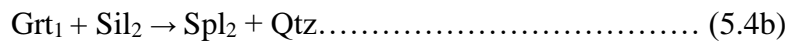
$$\text{Crn}_1 + \text{Grt}_1 \rightarrow \text{Spl}_2 + \text{Sil}_2 \dots \dots \dots (5.3)$$

Growth of fine vermicular to acicular Spl (Spl₃) within Grt₁ in association B (Fig. 5.1l) possibly occurred subsequent to reaction (5.3). Similar texture has been reported earlier by Das et al. (2006) who noted that vermicular spinel grains are restricted in the zone of sillimanite inclusions within porphyroblastic garnet. In such a case, pseudomorphic transformation of Sil inclusions (Sil₁) by Spl₃ may occur through a possible reaction



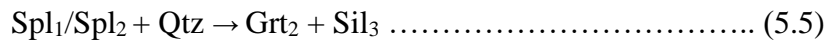
Tiny Qtz grains are present within the same Grt₁ host where Spl (Spl₃) is present. It is, however, difficult to constrain whether those Qtz grains are produced by reaction (5.4a) or were present beforehand.

The skeletal intergrowth of Spl₂ (hercynite: 70-72 mole%) and quartz replacing Grt₁ (almandine: 68-70 mole%) in the matrix (Fig. 5.1f) can be explained by the same reaction

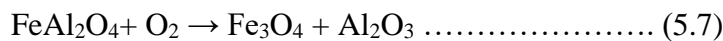
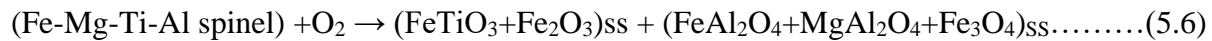


Reaction (5.4b) is responsible for occurrence of Qtz in the matrix in both the associations. The Spl grain (Spl₂) produced by reaction (5.3) and (5.4b) is genetically and compositionally different (Fe-Mg-Al spinel) than the Spl₁ grains (Fe-Mg-Ti-Al spinel) produced by reaction

(5.1). Reactions (5.1), (5.3) and (5.4b) indicate that the mineral assemblage of the peak M₂ stage was Spl₁/ Spl₂ + Sil₂ + Grt₁ + Qtz. Subsequently, the rock witnessed retrogressive metamorphism (M_{2R}) during which several reaction textures developed. The most common one is the double-layered corona of Grt₂ (almandine: 69-77 mole % in association A, and 68-71 mole% in association B) and Sil₃ separating Spl₂/Spl₁ from Qtz grains in the matrix (Figs. 5.1f, g). This particular texture indicates the reversal of reaction (5.4b).

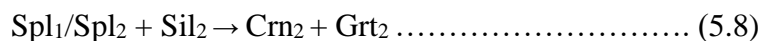


This reaction occurs during near-isobaric cooling at the retrograde stage (similar to M_{2R} in the present study) as inferred from many aluminous granulites of the EGB (Sengupta et al., 1991; Dasgupta et al., 1995; Bose et al., 2000). At this stage, Spl₁ solid solution was also decomposed to Ilm (Ilm₂), Mag and locally Crn (Crn₃) by several oxy-exsolution reactions



As the coexisting Spl-Ilm (bipartite), Spl-Ilm-Mag (tripartite) and Spl-Mag-Crn (tripartite) grains are enveloped by the Sil (Sil₃) corona, the reactions (5.6) and (5.7) must have occurred subsequent to the reaction (5.5).

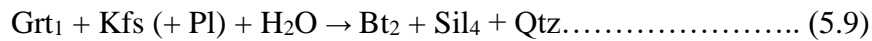
Corona of Grt₂ around Sil₂ and the presence of Crn₂ within Grt₂ and Spl₁/Spl₂ possibly suggests reversal of reaction (5.3) during cooling.



In this reaction, presence of Grt₂ corona around Sil₂ (Fig. 5.6e) confirms that Spl (Spl₁ and/or Spl₂) must have been present as reactant phase as no other Fe-Mg bearing phases were present at this stage. Presence of Spl₁/Spl₂ in the vicinity of Sil₂ grains also corroborates this fact. However, Crn (Crn₂) produced during this reaction are vermicular or granular in shape. In the latter case,

fine granules of Crn₂ nucleated preferably along the fractures within Spl₁ and/or Spl₂ (inset of Fig. 5.6e).

Bt (Bt₂) (X_{Mg}: 0.63-0.67 in the association A and 0.46-0.58 in the migmatitic felsic gneiss) appeared late on Grt₁ in the association A as well as in the migmatitic felsic gneiss (Almandine: 78-81 mole%). This Bt₂ is often intergrown with fine acicular Sil (Sil₄) and the Bt₂+Sil₄ assemblage also defines the S₄ foliation both in the aluminous granulite (Association A) and the migmatitic felsic gneiss. This assemblage was possibly formed by the following reaction at the late M_{2R} stage of metamorphism.



It is notable that the association B is devoid of any retrograde Bt. The reason behind this can be either absence of Kfs in the association B, or availability of limited H₂O from the outgoing melt. Another important feature is that both Bt₁ and Bt₂ contain high amount of F, at places. Such a high amount of F in Bt₁ could be the result of partition of F into these biotite grains during consumption of the same in course of melting reactions. However, this process is not responsible for high amount of F in Bt₂ which is presumably produced during back reaction involving the melt and the mineral phases containing Fe and Mg (Grt and Spl in the present case) similar to one suggested by Motoyoshi and Hensen (2001). Similar features have also been documented from the central part of the EGB by Bose et al. (2005) who considered high F content was responsible for stabilization of biotite-bearing assemblages up to 950°C at the mid- to deep crustal level.

5.5 Geothermobarometry of aluminous granulite

Conventional P-T estimation of different stages is fraught with difficulty due to the non-appearance of temperature sensitive minerals like orthopyroxene and cordierite in the assemblage. Nevertheless, attempts have been made to estimate the thermobaric conditions from the observed mineral assemblages and the result is summarized in Table 5.3. The near-peak (M_2) temperature and the pressure were constrained respectively from the Spl_1 - Sil_3 - Grt_2 -Qtz assemblage (Nichols et al., 1992) and Grt_1 - Spl_2 - Sil_2 -Qtz assemblage (Bohlen et al., 1986) of aluminous granulite. Using the thermometer of Nichols et al. (1992), the temperatures of 938-964°C and 917-945°C were estimated from associations A and B respectively at an assumed pressure of 8 kbar. These temperatures estimates represent reset values due to late-stage Fe-Mg exchange. The Bohlen et al. (1986) barometer yields 8.0-8.2 kbar pressure. Activities of Grt_1 and Spl_1 were calculated using the program *A-X* developed by Holland and Powell (1998). Using the Grt_1 - Crn_1 - Spl_2 - Sil_2 barometer (Shulters and Bohlen, 1989), the pressure was estimated to be 7.8-8.1 kbar, which is the best estimate for the pre- M_2 stage of metamorphism when Crn_1 was stable. The temperature for the retrograde stage (late M_{2R} stage of metamorphism) was constrained by Bt_2 coexisting with Grt_1 in association A of the aluminous granulite. Using the garnet-biotite Fe-Mg exchange thermometer of Ganguly et al. (1996) the temperature was estimated to be 643-679°C for the association A of aluminous granulite. Additionally using the Ti-in-biotite thermometer (Henry et al., 2005), the temperature was calculated to be up to 790°C for the same association of aluminous granulite. For the migmatitic felsic gneiss sample, the estimated peak pressure is 7.4-8.6 kbar using the garnet-aluminosilicate-silica-plagioclase barometer (Newton and Haselton, 1981). It is important to note that the higher and lower pressure values were estimated using the core and rim compositions respectively of porphyroblastic Grt grains. The

temperature for the retrograde stage (late M_{2R} stage of metamorphism) was constrained by Bt coexisting with Grt in the migmatitic felsic gneiss. Using the garnet-biotite Fe-Mg exchange thermometer of Ganguly et al. (1996) the temperature was estimated to be 468-680°C for the migmatitic felsic gneiss. The higher (e.g. 680°C) and lower (e.g. 468°C) temperatures were estimated using the core and rim compositions of garnet. In the same rock, Ti-in-biotite thermometer (Henry et al., 2005) was utilized which documents temperature up to 713°C. The geothermobarometric result of the aluminous granulite and the migmatitic felsic gneiss is summarized in Table 5.3.

5.6 Phase diagram modeling

To understand the pre peak (pre- M_2) to post-peak (M_{2R}) evolutionary history of the aluminous granulite, phase diagram modeling was done using the program *Perple_X* ver 6.7.5 (Connolly and Pettrini, 2002; Connolly, 2005, 2009). Internally consistent thermodynamic dataset of Holland and Powell (1998) was utilized for construction of the phase diagrams. Since the aluminous granulite developed broadly similar mineral associations and reaction textures, only one representative sample containing the minerals of association B was chosen for phase diagram modeling. As mentioned earlier, association B represents a restitic character due to extraction of melt with low modal abundance of quartz and absence of feldspar. Although only a few theoretical analyses are available (McDade and Harley, 2001; Kelsey et al., 2005), experimental data on phase relationships for Mg-Fe-Al rich Si-undersaturated bulk rock is limited (e.g. Shulters & Bohlen, 1989). The bulk composition for phase diagram modeling was calculated using the method of effective bulk composition (Stuwe, 1997). For this, mineral modes were initially calculated from four different micro-domains of the representative section

of association B that show the maximum modal variations. This was done to eliminate the heterogeneity of the mineral distribution within the aluminous layers. The average modal composition was calculated from the results of the four micro-domains. Average mineral compositions were integrated with modal values to get the suitable bulk.

Phase diagram calculation was done in the FeO-MgO-Al₂O₃-SiO₂-TiO₂-MnO-O₂ (FMASTMnO) system for association B. The phase diagram in the system Na₂O-CaO-K₂O-FeO-MgO-Al₂O₃-SiO₂-H₂O-TiO₂-MnO-O₂ (NCKFMASHTMnO) was also calculated to account the evolution of association A where matrix biotite and melt relics are present as additional phases. To retrieve the bulk composition of the latter association, 10 modal% lost melt composition was added with the calculated bulk composition. The modal% of the melt was estimated from the abundance of quartz and feldspar grains showing melt-crystallizing textures for which a value of 10% was taken as the maximum. The melt composition was taken from the average Proterozoic S-type granite (Chappell and White, 1983). To constrain the oxygen fugacity, the approach outlined by Korhonen et al. (2012) and Kelsey and Hand (2015) was adopted. Accordingly, a T-O₂ phase diagram was constructed at 8 kbar (Fig. 5.2a) to show the stability fields of the observed assemblages with changing O₂ values. Figure 5.2a shows that corundum- and quartz-bearing assemblages stabilize with 0.56 wt% and 0.65 wt% of O₂ respectively within the temperature range of 700-1100°C. Therefore, a median O₂ value of 0.3 wt% was chosen to construct the P-T phase diagram. Solid solution models for garnet, cordierite, melt and orthopyroxene were taken from the database of Holland and Powell (1998, revised in 2003), while the solution model of spinel was taken from White et al. (2002). A few ilmenite grains occur without spinel, but it is difficult to decide whether these are discrete phases (stable with spinel as the phase diagram suggests) or formed due to granular exsolution of the erstwhile

spinel solid solution (Waters, 1991). For biotite, the deprotonation model of White et al. (2007) was used.

The resulting P-T phase diagram for association B is presented in figure 5.2b which shows the stability of garnet-spinel-sillimanite-corundum-ilmenite and garnet-spinel-sillimanite-ilmenite-quartz assemblages within a wide pressure and temperature range. The former mineral assemblage was stable up to 800°C temperature at about 8 kbar pressure during the pre-M₂ stage. The latter assemblage was stable at the peak-M₂ stage above 950°C temperature at a similar pressure. These two assemblages are separated by a high-variance assemblage of garnet-spinel-sillimanite-ilmenite (striped area in the Fig. 5.2b). Both corundum and quartz are absent in this field and the transformation of pre-M₂ to peak-M₂ assemblages would require approximately 150°C increase in temperature through this field. Alternatively, switching of these two assemblages can also be controlled by SiO₂ as demonstrated in the T-SiO₂ diagram (Fig. 5.2c) which shows that the same change can occur by increasing the amount of SiO₂ at a much lower temperatures. Such a process could be speculated as the Si-undersaturated domains are hosted by quartzofeldspathic domains which might have supplied SiO₂. The transformation in this case would be near-isothermal and follow a path through a very narrow temperature interval of approximately 780 to 820°C. Given the uncertainty in calculating the effective bulk composition of the chosen system, this interval is too specific. The P-T phase diagram (Fig. 5.2b), on the other hand, indicates that the quartz-bearing peak-M₂ assemblage becomes stable only above 950°C (at 8 kbar pressure), and the transformation of corundum-bearing pre-M₂ to quartz-bearing peak-M₂ assemblage can occur due to increase in temperature without changing the SiO₂ content. This shift in mineral assemblages, therefore, occurred due to heating along the prograde path. Thus the spinel + quartz assemblage may stabilize from the garnet + corundum assemblage

in a Si-undersaturated pelitic bulk which was deduced from textural criteria and mineral reactions (5.3) and (5.4b). Modal isopleths of spinel in P-T phase diagram show that the proportion of spinel increases from the pre-M₂ to the peak-M₂ stage (Fig. 5.2b).

Phase diagram with calculated bulk after addition of traces of melt and K-feldspar composition is represented in figure 5.3. It shows stability of the mineral assemblage garnet + spinel + sillimanite + ilmenite + quartz + melt defining the peak-M₂ stage of association A. This peak assemblage is corundum-free which was stabilized by increasing temperature from a corundum-bearing assemblage. This transformation occurred through a 200°C temperature window where both corundum and quartz are absent as demonstrated in the case of association B. Interestingly, K-feldspar is not a stable phase in the peak assemblage (Fig. 5.3) although it is physically present in association A. It suggests that although K-feldspar was produced as a peritectic phase (reaction 5.1) during prograde stage, it shows metastable relation with the peak assemblage. The peak M₂ assemblage of garnet+ spinel+ sillimanite + ilmenite + quartz + melt stabilizes at approximately 1000°C assuming the pressure of 8 kbar. It is important to note that the biotite-out curve would shift towards higher temperature if the effect of F is considered (Dooley and Patino Douce, 1996; Bose et al., 2005).

Both associations produced M_{2R} assemblages as a result of cooling from the peak-M₂ stage, albeit with a variety of minerals and their textural modes. Corona of Sil₃ and Grt₂ around Spl₁-Ilm₂ (reaction 5.5) provide the evidence of cooling. Corona of Grt₂ around Sil₂ and presence of Crn₂ in Spl₁ and Grt₁ (reaction 5.8) also corroborate this. On further cooling, Bt-bearing assemblage is produced in association A due to rehydration during the late M_{2R} stage. Results of the phase diagram modeling demonstrate a heating-dominated prograde path followed by a cooling-dominated retrograde P-T trajectory. Sengupta et al. (1999) constructed a KFMASH

petrogenetic grid involving corundum and quartz and showed that the stability of garnet-corundum-spinel-sillimanite occurs exclusively at pressure $> P_{[\text{Spr, Opx, Qtz}]}$ (i.e. above 7 kbar). Results in this study also show that the $\text{Gr}_1\text{-Crn}_1\text{-Spl}_1\text{-Sil}_2$ stability field occurs only at high pressure (>8.4 kbar, Fig. 5.3). Figure 5.3 also shows that the same assemblage can be stable up to ~ 10.2 kbar pressure. Using phase diagram modeling, it is thus demonstrated that the aluminous granulite evolved through a P - T path which remained isobaric during the prograde and the retrograde stages and must lie above 8.4 kbar. However, the maximum stability of the prograde assemblage may shift up to $\sim 900^\circ\text{C}$ due to high F content of biotite.

5.7 Summary

1. Geothermobarometry and phase diagram modeling suggest that the aluminous granulite was metamorphosed at UHT condition (M_2 : $\sim 1000^\circ\text{C}$) at ~ 8 kbar.
2. Textural characters and phase diagrams additionally indicate that spinel+quartz-bearing assemblage (M_2) became stable at UHT from corundum-bearing mineral assemblage (pre- M_2) in aluminous granulite.
3. Garnet and sillimanite corona developed in aluminous granulite in response to near-isobaric cooling (M_{2R}) following UHT metamorphism. Continued cooling produced biotite-bearing mineral assemblages (late M_{2R}) in aluminous granulite and migmatitic felsic gneiss.
4. The P - T path remained isobaric during the prograde and the retrograde stages.